Journal of Developmental Biology

MDPI

Article

COMMD10 Is Essential for Neural Plate Development during Embryogenesis

Khanh P. Phan [1], Panayiotis Pelargos [1], Alla V. Tsytsykova [1], Erdyni N. Tsitsikov [1], Graham Wiley [2], Chuang Li [3], Melissa Bebak [3] and Ian F. Dunn [1,*]

[1] Department of Neurosurgery, University of Oklahoma Health Sciences Center, Oklahoma City, OK 73104, USA; khanh-phan@ouhsc.edu (K.P.P.); panayiotis-pelargos@ouhsc.edu (P.P.); alla-tsytsykova@ouhsc.edu (A.V.T.); erdyni-tsitsikov@ouhsc.edu (E.N.T.)
[2] Clinical Genomics Center, Oklahoma Medical Research Foundation, Oklahoma City, OK 73104, USA; graham-wiley@omrf.org
[3] Genes & Human Disease Research Program, Oklahoma Medical Research Foundation, Oklahoma City, OK 73104, USA; chuang-li@omrf.org (C.L.); melissa-bebak@omrf.org (M.B.)
* Correspondence: ian-dunn@ouhsc.edu

Abstract: The COMMD (copper metabolism MURR1 domain containing) family includes ten structurally conserved proteins (COMMD1 to COMMD10) in eukaryotic multicellular organisms that are involved in a diverse array of cellular and physiological processes, including endosomal trafficking, copper homeostasis, and cholesterol metabolism, among others. To understand the role of COMMD10 in embryonic development, we used *Commd10*$^{Tg(Vav1\text{-}icre)A2Kio}$/J mice, where the *Vav1-cre* transgene is integrated into an intron of the *Commd10* gene, creating a functional knockout of *Commd10* in homozygous mice. Breeding heterozygous mice produced no COMMD10-deficient *(Commd10*^{Null}*)* offspring, suggesting that COMMD10 is required for embryogenesis. Analysis of *Commd10*^{Null} embryos demonstrated that they displayed stalled development by embryonic day 8.5 (E8.5). Transcriptome analysis revealed that numerous neural crest-specific gene markers had lower expression in mutant versus wild-type (WT) embryos. Specifically, *Commd10*^{Null} embryos displayed significantly lower expression levels of a number of transcription factors, including a major regulator of the neural crest, *Sox10*. Moreover, several cytokines/growth factors involved in early embryonic neurogenesis were also lower in mutant embryos. On the other hand, *Commd10*^{Null} embryos demonstrated higher expression of genes involved in tissue remodeling and regression processes. Taken together, our findings show that *Commd10*^{Null} embryos die by day E8.5 due to COMMD10-dependent neural crest failure, revealing a new and critical role for COMMD10 in neural development.

Keywords: COMMD10; Sox10; neural crest; embryonic development

check for updates

Citation: Phan, K.P.; Pelargos, P.; Tsytsykova, A.V.; Tsitsikov, E.N.; Wiley, G.; Li, C.; Bebak, M.; Dunn, I.F. COMMD10 Is Essential for Neural Plate Development during Embryogenesis. *J. Dev. Biol.* **2023**, *11*, 13. https://doi.org/10.3390/jdb11010013

Academic Editors: Claire Chazaud and Simon J. Conway

Received: 29 January 2023
Revised: 12 March 2023
Accepted: 14 March 2023
Published: 16 March 2023

1. Introduction

Endosomes are intracellular lipid bilayer organelles that regulate the trafficking of biological cargo between the plasma membrane and other subcellular compartments, including the *trans*-Golgi network and lysosomes. Following endocytosis, transmembrane proteins undergo sorting to be recycled back to the cell surface or sent for degradation in lysosomes. Cell surface recycling is essential for membrane receptor maintenance and is executed by two distinct protein complexes: Retromer and Retriever (reviewed in [1]). Each of these recycling complexes associates with other multi-protein structures, such as the Wiscott-Aldrich and Scar Homolog (WASH) complex and the COMMD/CCDC93/CCDC22 (CCC) complex [2,3]. Mutations in these multi-protein complexes are increasingly associated with human pathologies, including neurodegenerative and developmental disorders [4–7].

The COMMD (copper metabolism MURR1 domain)-containing subunit of the CCC complex includes several COMMD family proteins [1]. All members of this family share

a unique C-terminal motif termed a COMM domain, which fosters homo- and heterodimerization of COMMD proteins and facilitates interactions with CCDC22 and CCDC93. On the other hand, the N-terminal region is unique in each COMMD protein, suggesting their diverse functions [8]. The first identified member of this family, COMMD1, was discovered to be mutated in Bedlington terriers with copper toxicosis [9]. Subsequently, COMMD1 was demonstrated to regulate the endosomal sorting of the copper transporter ATP7A [2]. COMMD1 also participates in the downregulation of nuclear factor kappa B (NF-κB)-dependent transcription [10,11].

The analysis of *Commd10* conditional knockout mice with targeted deficiency to myeloid cells and macrophages demonstrated its direct role in propagating phagolysosomal maturation and clearing of monocyte-driven inflammation [12] and infection [13]. However, *Commd10* is ubiquitously expressed, suggesting its role in other tissues [14,15]. Here, we examine the role of COMMD10 in the embryonic development of mice with a disrupted *Commd10* gene.

2. Materials and Methods

2.1. Mice

Commd10^{Het} mice were bought from the Jackson Laboratory (B6.Cg-Commd10$^{Tg(Vav1\text{-}icre)A2Kio}$/J, Stock # 008610) [16]. Wild-type (WT) and *Commd10*^{Null} embryos were generated by interbreeding of *Commd10*^{Het} littermates. Animals were housed and bred in a specific pathogen-free animal facility and fed a standard diet. All mouse breeding and procedures were carried out according to the laboratory animal protocol approved by the IACUC. Animal genotyping was based on the detection of the intact *Commd10* allele and *iCre* by real-time PCR using a DuPlex PCR approach with the following TaqMan assays:

Commd10-Fwd: CGGGTCTTCCCATCTCATTT
Commd10-Rev: TCAACTGGTTAGTCGGGATTG
Commd10 Probe: CAGACACACCCAGAGGCTCATTCATT
iCre-Fwd: TGGGCATTGCCTACAACA
iCre-Rev: ATCAGCATTCTCCCACCATC
iCre Probe: CGCATTGCCGAAATTGCCAGAATCA

2.2. Embryological Analysis

In order to harvest embryos at specified embryologic stages, timed pregnancies were set up by breeding *Commd10*^{Het} mice. The embryos were considered 0.5 days post coitus (dpc) at noon on the day of detection of the vaginal plug. At embryonic days 8.5 (E8.5), E9.5, and E10.5, females were euthanized and embryos extracted. Embryonic genotyping was performed on genomic DNA purified from yolk sacs. Whole embryo images were obtained at total magnifications of 15× and 45× (combination of magnifications of 1.5× and 4.5× objective lens with 10× ocular lens) using an AmScope microscope with a MU1003 digital camera and AmScope software (AmScope).

2.3. Western Blot Analysis

Whole embryos were lysed in 1× Laemmli Sample Buffer (BIO-RAD, Hercules, CA, USA, 1610747) with 50 mM DTT, mixed with glass beads, and shaken in an Eppendorf shaker at 2000 RPM at 85 °C for 10 min. Samples were run on a 4–15% Mini-PROTEAN® TGX™ Protein Gel (BIO-RAD, 4561083); transferred to nitrocellulose membranes, which were blocked with Blotting-Grade Blocker (BIO-RAD, 1706404); and probed with anti-COMMD10 (Fisher Scientific, Waltham, MA, USA, PIPA531868; RRID: AB_2549341), anti-COMMD1 (Fisher Scientific, PIPA598616; RRID: AB_2813229), or anti-Sp1 antibody (Sigma-Aldrich, St. Louis, MO, USA, 07-645). Goat anti-rabbit IgG, HPR-linked (Cell Signaling Technologies, Danvers, MA, USA, 7074) was used as a secondary antibody. Sp1 levels were measured as loading controls.

2.4. RNA Extraction

WT and *Commd10*^{Null} embryos at days E8.5, E9.5, and E10.5 were extracted from yolk sacs and immediately placed in Invitrogen™ RNA*later*™ Stabilization Solution (Fisher Scientific, AM7023). They were kept at 4 °C for 24 h and transferred to −80 °C for long-term storage before RNA extraction. Total RNA was extracted using the RNeasy Plus Micro Kit (QIAGEN, Hilden, Germany, 74034) and QIAshredder (QIAGEN, 79656) according to the manufacturer's instructions.

2.5. RNA-seq and Differential Expression (DE) Analysis

Total RNA purified from WT and *Commd10*^{Null} embryos at E8.5, E9.5, and E10.5 was subjected to full transcriptome sequencing. At least three biological repeats were carried out for each condition. 3′-end RNA libraries were made using the Lexogen QuantSeq 3′ mRNA-seq Library Prep Kit FWD for Illumina. Sequencing was performed from single-end 75bp on an Illumina NextSeq High Output.

Post-sequence reads were quality-filtered for length and contaminants and were trimmed for Illumina adapters using BBDuk [17]. The resulting reads were pseudo-aligned to coding regions of the mouse reference genome (mm10) using STAR [18]. Gene annotation was performed via the R package biomaRt [19]. Differential expression was calculated using the Wald test implemented in the R package DESeq2 [20]. Significantly differentially expressed genes were defined as those that had both an absolute log2Fold change ≥ 1 and a false discovery rate (FDR) adjusted p-value ≤ 0.05 for each comparison independently.

2.6. Quantitative PCR (RT-qPCR)

Whole embryo total RNA was used to measure gene mRNA levels by real-time qPCR. Reverse transcription and cDNA amplification were performed in one tube using qScript™ XLT One-Step RT-qPCR ToughMix®, Low ROX™ (VWR Quanta Biosciences™, Beverly, MA, USA, 95134) on an Applied Biosystems 7500 Fast Real-Time PCR System (Fisher Scientific). Sample reactions were run in 3–6 replicates. Each mRNA analysis was run in a DuPlex PCR reaction with *Gapdh* as an internal control. Standard curves for each gene were run to verify the linear range of amplification. Input RNA was kept under 200 ng per reaction to stay within the linear range for *Gapdh* levels.

All data were analyzed in Microsoft Excel with the built-in analysis methods. TaqMan assays used for RT-qPCR are as follows (m–mouse assays):

mGapdh-Fwd: CCTGTTGCTGTAGCCGTATT
mGapdh-Rev: AACAGCAACTCCCACTCTTC
mGapdh Probe: TTGTCATTGAGAGCAATGCCAGCC
mSox10-Fwd: GCTATTCAGGCTCACTACAAGA
mSox10-Rev: GGACTGCAGCTCTGTCTTT
mSox10 Probe: ATGTCAGATGGGAACCCAGAGCAC

3. Results and Discussion

To examine the role of COMMD10 in embryonic development, we used B6.Cg-*Commd10*$^{Tg(Vav1\text{-}icre)A2Kio}$/J mice (Jackson Laboratory; stock #008610). In these mice, the *Vav1-iCre* transgene is integrated into the intron between exons 5 and 6 of the *Commd10* gene on chromosome 18 (Figure 1a) [16]. The insertion resulted in a functional knockout of *Commd10* in homozygous (*Commd10*^{Null}) mice [21]. Crossbreeding of *Commd10* heterozygous (*Commd10*^{Het}) littermates produced no *Commd10*^{Null} newborn mice, while WT and heterozygous genotypes were born at the expected Mendelian ratio (Figure 1b). These results are consistent with those of a viability primary screen phenotypic assay performed on another *Commd10* mutant mouse strain (*Commd10*$^{tm1a(EUCOMM)Wtsi}$) from the EUCOMM consortium (strain #EPD065) at https://www.mousephenotype.org/data/genes/MGI:1916706 (accessed on 17 July 2022). However, the phenotype of these mice has not been reported in the literature. Thus, the essential role of COMMD10 in embryonic development was confirmed by using two different mouse strains with deficient COMMD10 expression.

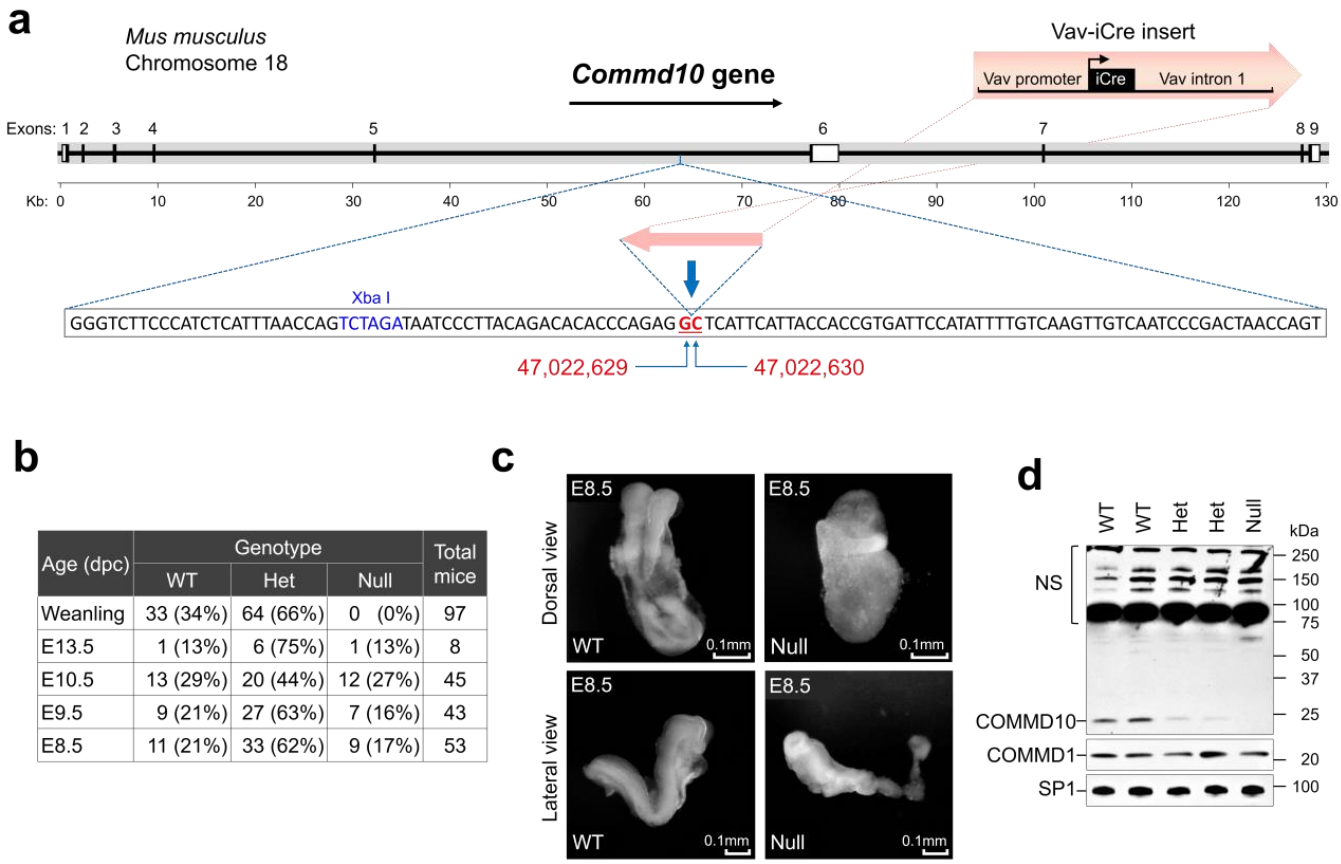

Age (dpc)	Genotype			Total mice
	WT	Het	Null	
Weanling	33 (34%)	64 (66%)	0 (0%)	97
E13.5	1 (13%)	6 (75%)	1 (13%)	8
E10.5	13 (29%)	20 (44%)	12 (27%)	45
E9.5	9 (21%)	27 (63%)	7 (16%)	43
E8.5	11 (21%)	33 (62%)	9 (17%)	53

Figure 1. COMMD10 deficiency results in embryonic lethality. (**a**) Schematic drawing (up-to-scale) of the *Commd10* gene on mouse chromosome 18 shown as a thick grey line. Its direction of transcription is indicated by the black arrow above. Coding exons are represented as thin black boxes. Noncoding 5′- and 3′-untranslated regions are shown as open boxes. The Vav-iCre cassette sketch is shown above the track. The sequence around the Vav-iCre cassette insertion site is shown below the gene scheme in an inset window. Flanking the cassette, GC nucleotides are marked by red bold underlined font and indicated by blue arrows. Their exact positions in the genome are designated by numbers from Reference GRCm39 C57BL/6J below the sequence window. (**b**) Genotyping analysis of offspring of heterozygous *Commd10*^{Het} mice (Het) mating. *Commd10*^{Null} (Null) mice had never been born but embryo genotypes show the expected Mendelian distribution. (dpc): days post-coitus. (**c**) Morphological analysis of WT and *Commd10*^{Null} (Null) embryos at E8.5 in dorsal (top panels) and lateral (bottom panels) views. (**d**) Western blot analysis of whole embryo lysates and anti-COMMD10 or anti-COMMD1 antibodies, as indicated. Anti-SP1 antibody was used as the loading control. NS: non-specific bands.

E8.5 *Commd10*^{Null} embryos were visually abnormal and displayed abnormal neural plate morphology and growth retardation, but still remained comparable in size and yielded a comparable amount of RNA for analysis (Figure 1c). E9.5 and E10.5 mutant embryos showed progressive degradation and signs of tissue resorption (Figure S1a). Western blot analysis of E8.5 embryo lysates demonstrated lower levels of COMMD10 protein in *Commd10*^{Het} embryos and its complete absence in *Commd10*^{Null} embryos compared with WT embryos (Figure 1d).

To examine the root cause of the developmental failure of *Commd10*^{Null} embryos, we carried out comparative transcriptome analyses of mutant and WT embryos (Figure S1b). Figure 2a shows the gene expression principal component analysis (PCA) plot. The cluster of WT samples on E8.5 appears stretched compared with other clusters, indicating some variability among WT samples on that day. The rest of the clusters are tight without any overlap. Importantly, the direction of embryonic development from E8.5 through E10.5

is reflected in the WT cluster distribution on the PCA plot (WT arrow). Interestingly, *Commd10*^{Null} E8.5 and E9.5 clusters are located on opposite sides of the WT E8.5 samples. Importantly, both of these clusters are far from each other and from E10.5 samples (Figure 2a, C10_Null arrow). This segregation pattern suggests that the divergence point between WT and *Commd10*^{Null} embryos took place not long before day E8.5. Thus, the *Commd10*^{Null} E8.5 transcriptome represents an inflection point in embryogenesis from development to tissue resorption.

Figure 2b shows a volcano plot visualizing differentially expressed genes (DEGs) in WT vs. *Commd10*^{Null} embryos at E8.5 and displaying wide areas of scattered genes on both sides of the y-axis. We sorted all significant DEGs by the absolute value of log2FoldChange and chose the top 100 DEGs to plot on a heatmap (Figure 2c). Among these top 100 DEGs, only 15 were upregulated in *Commd10*^{Null} embryos, and the 85 remaining genes were downregulated in contrast to those in WT embryos. Interestingly, the 85 DEGs that are downregulated in mutant embryos include 20 transcription factors, at least 11 cytokines/growth factors/cell surface receptors, and 30 genes with unknown function. The rest of these DEGs encode structural proteins, modifying enzymes, and proteins involved in ion channel function, cell adhesion, and other metabolic cellular processes.

To find the specific embryonic lineage where each of these DEGs is expressed, we searched a single-cell molecular map of mouse gastrulation and early organogenesis at https://marionilab.cruk.cam.ac.uk/MouseGastrulation2018/ (accessed on 2 September 2022) [22]. This interactive atlas demonstrates specific mRNA expression profiles during mouse embryonic development between E6.5 and E8.5. As shown in Figure 2d, *Commd10* is broadly expressed in all lineages during embryogenesis. The top most significantly (461-fold) downregulated gene in *Commd10*^{Null} embryos at E8.5 is Sox10, a transcription factor with a central role in neural crest development and maturation of glia [23]. We have also validated Sox10 mRNA expression in WT and *Commd10*^{Null} embryos at E8.5, E9.5, and E10.5 by RT-qPCR and found the highest Sox10 expression and the most drastic difference between the two genotypes at E8.5 (Figure S1d). In normal developing mouse embryos, Sox10 expression emerges after E8.0 almost exclusively in the neural crest (Figure 2d). The table in Figure 3a lists the top ten neural crest-specific markers according to the interactive atlas. Interestingly, six of those markers were differentially expressed in WT versus *Commd10*^{Null} embryos, suggesting that there is a defect in neural crest development in *Commd10*^{Null} embryos (Figures 2b–d and 3b). Moreover, a list of significant DEGs, which define the trajectory of neurogenesis, includes numerous transcription factors critical for neural plate development, starting from rostral neuroectoderm at E6.5 and subsequent development of caudal neuroectoderm, spinal cord, forebrain/midbrain/hindbrain, and neural crest by E8.5.

Besides Sox10, *Commd10*^{Null} embryos exhibit significantly lower expression of transcription factors Tfap2b [24,25], Nr2f1 [26], Msx3 [27], Dbx2 with Pax6 [28,29], Sox1 [30], Gbx2 [31], Zic1 [32], Pou3f2 [33–35], Prdm13 [36], Fezf1 [37], Six6 [38,39], Foxg1 [40], and Foxi2 [41] (Figure 3). They all participate in the early stages of central nervous system development. Also significantly downregulated in *Commd10*^{Null} embryos are genes encoding cytokines/growth factors involved in early embryonic neurogenesis, such as Ptn [42,43], Mdk [43,44], and Grem1 [45] (Figure 2b). In addition, transcription factors such as Meox2 [46], expressed in paraxial and somatic mesoderm, and Bhlha9 [47,48], expressed in surface ectoderm, are important for the expression of genes involved in signaling pathways essential for the formation and morphogenesis of somites and limbs in developing embryos (Figure 3). Taken together, these data are in agreement with the observation that WT embryos at E8.5 undergo continuous embryogenesis by means of cell proliferation, migration, and differentiation, particularly in the process of primary neurulation. This highly orchestrated process is defined by the expression of a number of transcription and growth factors that are coordinated in place and time. Significantly lower levels of these molecules in *Commd10*^{Null} embryos may result in the termination of embryonic development.

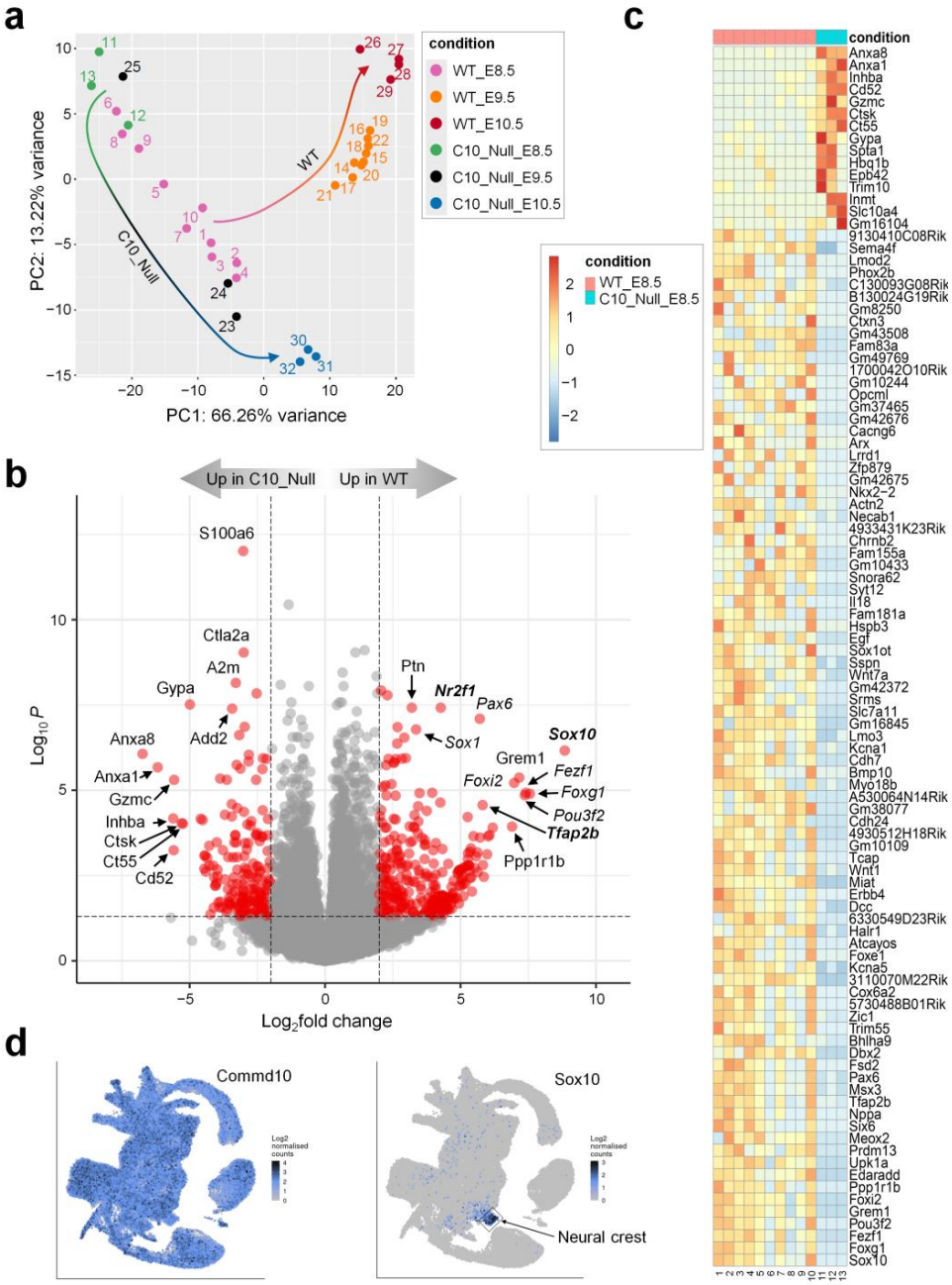

Figure 2. *Commd10*^{Null} embryos fail to develop beyond E8.5 due to impaired neural plate and neural crest development. (**a**) PCA plot of RNA-seq analysis in WT and *Commd10*^{Null} (C10_Null) embryos at E8.5, E9.5, and E10.5. Sample clusters are shown in different colors. Colored arrows show direction of cluster shifts through E8.5 to E10.5 developmental timeframe for both genotypes. Changing arrow colors correlate with the corresponding sample cluster in a timeframe. (**b**) Volcano plot of RNA-seq analysis visualizing significant DEGs in WT vs. *Commd10*^{Null} (C10_Null) E8.5 embryos: magnitude of change (x-axis) vs. statistically significant *p*-values (y-axis). Points that have a fold change less than 2 ($\log_2 = 1$) are shown in grey. Genes that are transcription factors are marked in italic font. Genes that are expressed in neural crest more highly than in any other cell type are shown in Bold font. (**c**) Heatmap of mRNA expression levels for top 100 significant DEGs in WT vs. *Commd10*^{Null} E8.5 embryos by RNA-seq. (**d**) Distribution of *Commd10* and *Sox10* mRNA expression in WT embryos during early embryogenesis in a single-cell molecular map [22]. Presented plots were generated on a single-cell molecular map of mouse gastrulation and early organogenesis at https://marionilab.cruk.cam.ac.uk/MouseGastrulation2018/ (accessed on 2 September 2022). The full legend annotating cell clusters by different colors and the schematic map are shown in Figure S1c.

a

Gene name	Base Mean	WT/*Commd10*^{Null} ratio Log2 FoldChange	FOLD Change	lfcSE	stat	pvalue	padj
Plp1	62.8535746	3.44284899	11	0.71495347	4.815486812	1.47×10^{-6}	8.18×10^{-5}
Tfap2b	253.522298	5.81454467	56	1.13994852	5.100708101	3.38×10^{-7}	2.71×10^{-5}
Sox10	115.340891	8.84772004	461	1.48791557	5.946385819	2.74×10^{-9}	6.87×10^{-7}
Foxd3							
Gadd45a	51.2775689	1.13150872	2	0.35251155	3.209848674	0.00132805	0.01295222
Gm12688							
Dlx2							
Nr2f1	976.274359	4.26986955	19	0.65336707	6.535177195	6.35×10^{-11}	3.80×10^{-9}
Enpp2	66.6155278	-1.50855407	3	0.35004661	-4.309580629	1.64×10^{-5}	0.00050336
Ncl							

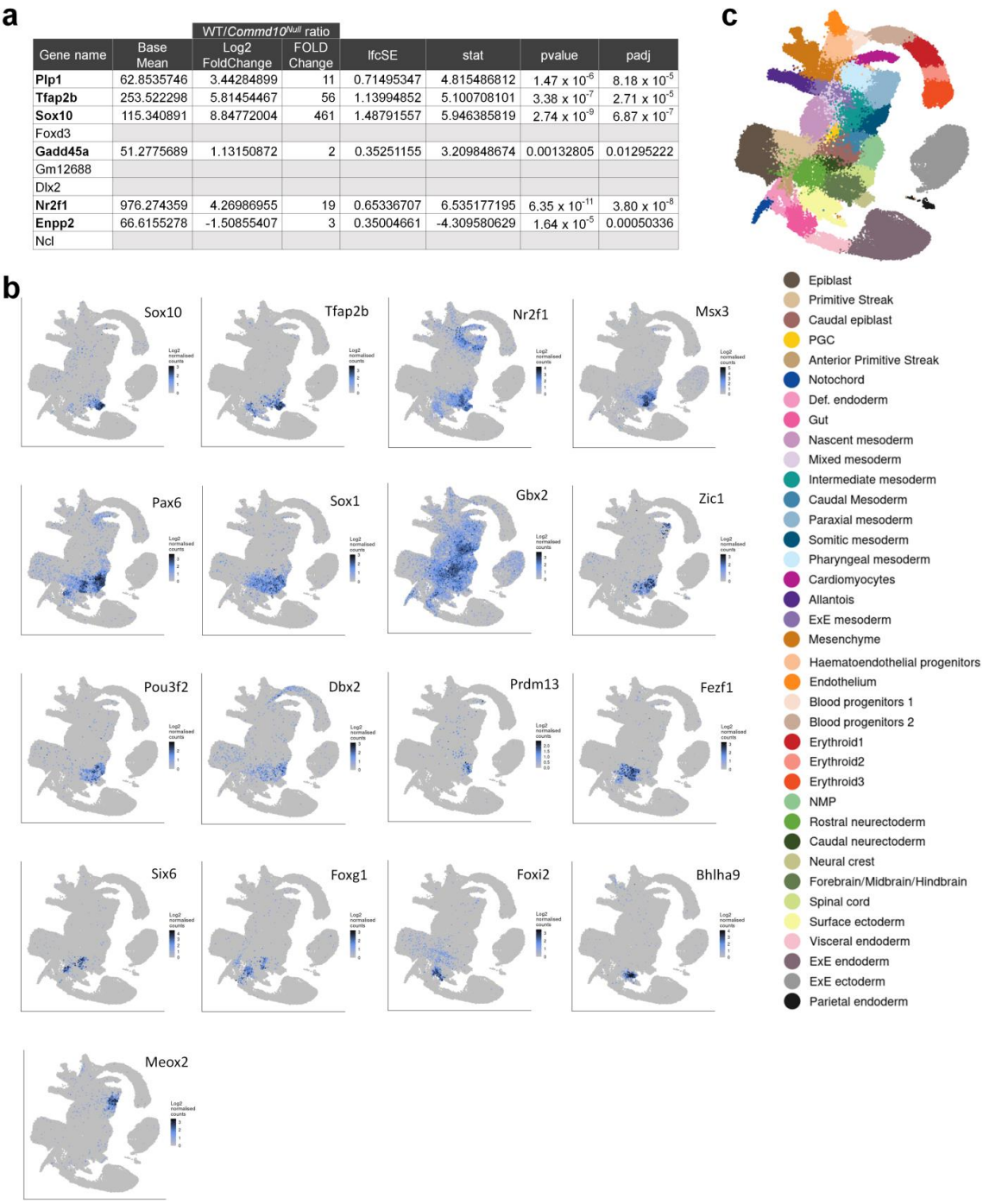

Figure 3. Six of the top ten neural crest-specific markers are differentially expressed in WT versus *Commd10*^{Null} embryos. (**a**) Table listing the top ten neural crest-specific markers, genes that are expressed in the neural crest more highly than in any other cell type. Six genes with differential expression in WT and *Commd10*^{Null} embryos are shown in bold font. (**b**) Tissue distribution of mRNA expression of different transcription factors in WT embryos during early embryogenesis in the molecular map of whole dataset, as described in (**c**). (**c**) Legend for (**b**) annotating cell clusters by different colors, and a single-cell molecular map of mouse gastrulation and early organogenesis [22] up to day E8.5 of embryogenesis. All presented plots were generated on a single-cell molecular map of mouse gastrulation and early organogenesis at https://marionilab.cruk.cam.ac.uk/MouseGastrulation2018/ (accessed on 2 September 2022).

On the other hand, there are no transcription factors or cytokine/growth factors among the top 15 DEGs upregulated in *Commd10*^{Null} embryos at E8.5 as compared with their WT littermates (Figure 2c). While some of these genes, such as Anxa8 and Anxa1 [49], are modestly expressed in notochord, caudal neuroectoderm, and neural crest of the WT embryos, most are not expressed in developing neural tissue (Figures 4 and 5). Instead, the majority of those genes are expressed in blood progenitors and erythroid tissue in particular (Gypa, Hbq1b, Epb42, Trim10 [50,51], Spta1). Interestingly, some of the upregulated DEGs in *Commd10*^{Null} embryos may be involved in tissue remodeling and regression. Granzyme C (Gzmc) is increased 48-fold in *Commd10*^{Null} embryos compared with WT, while Inhibin beta A chain (Inhba), a member of the inhibins/activins network of proteins, is increased 49-fold. Thus, embryonic cell death leading to tissue regression in E8.5 *Commd10*^{Null} embryos may be caused by two main events. The first event is a failure of the neural plate and neural crest processes due to a substantial deficiency of transcription factor Sox10, together with lower expression of other transcription factors and cytokines/growth factors involved in early embryonic neurogenesis. The second event is based on the increased expression of proteins with potential embryo resorption abilities.

To verify our conclusions further, we examined the expression of statistically significant DEGs with the top 25 gene markers representing each embryonic cell type present in the mouse embryo at E8.5 (Figure 5). A single-cell molecular map of mouse gastrulation and early organogenesis [22] lists 29 different cell/tissue types for the E8.5 mouse embryo. The gene analysis revealed that the majority of genes with low expression in *Commd10*^{Null} embryos are found in cells involved in early neural and heart development (Figure 5). Since recent studies demonstrated that neural crest cells develop into cardiomyocytes and contribute to heart development [52,53], gene expression deficiency in cardiomyocytes may be due to failed neural crest differentiation and/or cell migration.

We also performed gene functional enrichment analysis for the top 15–20 upregulated or downregulated DEGs using ToppGene Suite (https://toppgene.cchmc.org (accessed on 16 February 2023) [54]. We analyzed the top 20 genes downregulated in *Commd10*^{Null} embryos and came up with a "GO: Biological Process" list of positive regulation of RNA biosynthetic process, epithelium development, animal organ morphogenesis, and brain and head development. We also analyzed the top 15 genes upregulated in *Commd10*^{Null} embryos and selected the two top biological processes with the highest number of genes from the list: hemopoiesis and immune system development (Supplementary Tables).

Mice deficient in other members of the COMMD family, COMMD1 or COMMD9, were shown to be embryonically lethal. *Commd1*$^{-/-}$ embryos died between E9.5 and E10.5 due to defects in placenta vascularization [55]. Using genome-wide gene expression microarray analysis of embryonic RNA, the authors identified transcriptional upregulation of hypoxia-inducible factor 1 (HIF1) target genes in *Commd1*$^{-/-}$ embryos compared with their WT counterparts. Moreover, they demonstrated that COMMD1 may inhibit HIF1A stability and HIF1 activation by the physical association between the two proteins. Despite similarities in the timing of embryonic development failure between *Commd1*$^{-/-}$ and *Commd10*^{Null} embryos, there were no similarities in gene expression patterns in the present study. Only *Pfkp*, one of eighteen hypoxia-associated DEGs upregulated in *Commd1*$^{-/-}$ versus WT embryos, was slightly upregulated in *Commd10*^{Null} E8.5 embryos. Thus, the failure of *Commd10*^{Null} embryos to thrive appears to have different underlying reasons compared to *Commd1*$^{-/-}$ embryos.

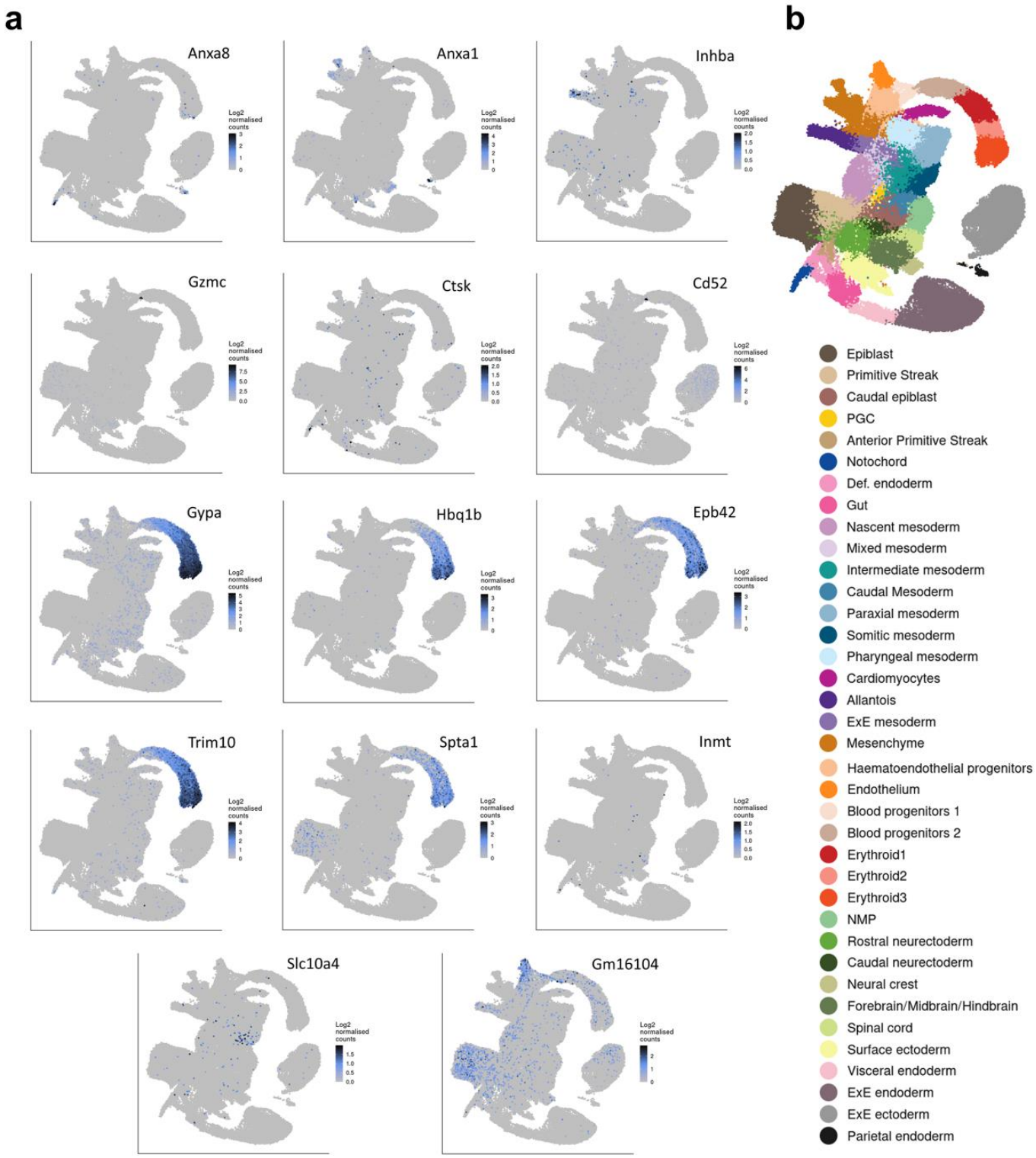

Figure 4. Tissue distribution of 14 genes significantly upregulated in *Commd10*^{Null} embryos on E8.5. (**a**) Single-cell molecular maps of mRNA expression in WT embryos for the top 14 genes significantly upregulated in *Commd10*^{Null} embryos on E8.5. (**b**) Legend for (**a**) annotating cell clusters by different colors, and a single-cell molecular map of mouse gastrulation and early organogenesis [22] up to day E8.5 of embryogenesis. All presented plots were generated on a single-cell molecular map of mouse gastrulation and early organogenesis. at https://marionilab.cruk.cam.ac.uk/MouseGastrulation2018/ (accessed on 2 September 2022) website.

	Parietal endoderm	ExE endoderm	Visceral endoderm	Definitive endoderm	ExE mesoderm	Caudal mesoderm	Intermediate mesoderm	Somitic mesoderm	Paraxial mesoderm	Rostral neuro-ectoderm	Surface ectoderm	Spinal cord	Forebrain/ Midbrain/ Hindbrain	Neuro-mesodermal progenitors	Neural crest	Pharyngeal mesoderm	Cardiomyocytes	Erythroid3	Erythroid2	Erythroid1	Blood progenitors2	Blood progenitors1	Endothelium	Haematoendothelial progenitors	Mesenchyme	Allantois	Gut	Notochord	Primordial germ cells
1	Creld2	Car7	Gde1	Tmem100	Hoxd1	Cdx4	Osr1	Pcdh19	Col26a1	Shisa2	Tacstd2	Fgfbp3	En1	Nkx1-2	Plp1	Alx1	Tnni1	Slc4a1	Cpne7	Gm15915	Rab27b	Il11ra1	Icam2	Etv2	Ahnak	Tmem119	Gpx2	Eif2b2	Rps29
2	Reep5	Aldob	Ddah2	Mfap4	Gm45357	Fgf17	Lhx1	Rftn1	Meox1	Sox11	Npnt	Mir124-2hg	Cntnap2	B230323A14Rik	Sox10	Rspo1	Nexn	Hemgn	Ndufaf4	Gata1	Plek	Alox5ap	Cldn5	Fev	Hand1	Prrx2	Pyy	Mnx1	Rps27a
3	P4ha2	Slc2a2	Ppil2	Lypd6b	Haglr	Evx1os	1110032F04Rik	Magi1	Ebf2	Gtf2h2	Sfn	Pcsk9	Cnih2	Hoxb9	Tfap2b	Aldh1a2	Sh3bgr	Cldn13	Fam72a	Mtg1	Ubash3b	Spi1	Cdh5	Hhex	Col1a2	Pcolce	Cldn8	Fam183b	Rpl18a
4	Lypla2	Smlr1	Pir	Alcam	Thy1	Greb1	Lhx1os	Tbx6	Tbx1	Emc8	Trp63	Hoxd4	Scrn1	Tesk2	Nr2f1	Dach1	Cap2	Gmpr	Abcb6	Vps51	Fermt3	Coro1a	Exoc3l4	Mmp9	Wisp1	Hoxa10	Tmem266	Hadha	Rps3a1
5	Ssr1	Pdzk1	Atf6b	Hoxb3os	Syt6	Ldha	Gpx6	Fgf9	Meox2	Tcp11l1	Foxi2	Stmn3	Jakmip2	Bicd1	Dlx2	Nxf3	Csrp3	Alas2	Hspe1	Naa10	Itga2b	Gimap5	Flt1	Tmem173	Col3a1	Pgf	Atp2c2	Colgalt1	Sub1
6	Wfdc1	Fxyd2	Serpina1a	Aco1	Sparcl1	Hoxc9	Zfp442	Tceal6	Tbx18	Nudt21	Upk3bl	Doc2a	Gdpd2	Hoxb8	A830082K12Rik	Fibin	Gm45123	Gypa	Tlk1	Csf2rb2	Fam212a	Cd34	Plvap	Swap70	Lum	Mbnl3	Tmem184a	Mocs1	Ifitm2
7	Mlec	Nrk	Cldn6	Cthrc1	Lhfpl3	Ppp1cc	2810474O19Rik	Dll1	Tgfbi	Dnajc15	Il17re	Zic1	Nuak2	Tm7sf2	Ngfr	Dusp14	Cnn1	Slc25a37	Ercc8	Wdr34	Rasgrp2	B9d2	Emcn	Anpep	Col5a2	Amer1	Gdpd1	Ahcy	Ifitm3
8	Klf5	Cldn2	Zdhhc20	Isg20	Epdr1	Wnt3a	Gm14226	Nkd2	9130410C08Rik	Wdr83os	Bhlha9	Gfra3	Mapk10	Spock3	Robo1	Pnliprp1	Unc45b	6030468B19Rik	Car1	Nudt9	Prkar2b	Ncf2	Gngt2	Tiam1	Postn	Smad6	Slc29a4	Cep44	Rpl35a
9	Tiprl	Creb3l3	Cldn3	Rom1	Scube3	Hoxb5os	Fut4	Aldoc	Itih5	Rbmx2	Wnt4	Msx3	Pipox	Olig3	Foxd3	Ttx1	Smarod3	Hbb-bs	Trmt61a	Tarsl2	Tgfb1	Hcls1	Sh3bp5	Lgals3bp	Colec11	Hoxa11	Rnf32	Gas2l1	Rplp2
10	Tmod3	0610005C13Rik	Cldn4	Rab38	Hoxd11	Etv4	Rps6kl1	2610528A11Rik	Ebf3	Fkbp4	Ntf5	Scube2	Car10	Adam23	Sdc3	Hs3st3a1	Ptges3l	Ermap	Mrps30	Smc2	Gfi1b	9-Sep	Rasip1	Lax1	Mab21l2	Stbd1	9030622O22Rik	Ppp2r5e	Pfdn5
11	Cdc42se2	Slc7a8	Epcam	Ptprd	Cacna2d3	Wnt5b	Mamdc4	Lor	Clmp	Rnps1	Cib2	BC030500	Garem2	Ifngr2	Crabp1	Kazald1	Ttn	Nxpe2	Wdr3	Steap3	Rgs10	Gpsm3	Elk3	Mmp17	Sult5a1	Twist2	Garnl3	Arf3	Rps7
12	Slc50a1	Tm4sf5	Fgfr1	Arhgap5	Ndnf	Notum	Nhlh2	Sv2b	Tnfaip6	Ap3s2	Epn3	Lrrtm3	AC153379.1	Camkv	Phactr1	Shisa3	Hspb7	Ube2l6	Timm8a1	Dynll2	F2r	Fam111a	Eng	C1ql2	Upk3b	Plac1	Zcchc18	D17Wsu92e	Rps10
13	P3h4	Soat2	Pdzk1ip1	Sox9	Oca2	Sapcd2	Nlrp6	Gpat3	Foxd2	Znhit1	Cbxn3	Grifin	Vgll3	Ncam1	B230312C02Rik	Cldn11	Fbxl22	Rhd	Cycs	Miip	Treml1	Gmfg	Abi3	Abhd6	Lrrn4	Vcam1	Cd164l2	Frat2	Rpl26
14	Serpinb6c	Morc4	Tmub1	Marcksl1	Magel2	Chst7	Xkr5	Tg	Cdh11	Thap11	Ppl	Olig2	Fam84a	Pof1b	Apod	Nr2f2	Myl1	Trim10	Lyar	Exosc5	Sla	Ppp1r18	Myzap	Gata2	Cbln1	Prdm6	Samd10	Trmt1l	Rps23
15	Aqp8	Esx1	Cers4	Sostdc1	Fgf10	Gm20052	4930525G20Rik	Chodl	Six2	Cad	Plxdc2	Neurog2	Flrt1	Chst11	Camk2b	Sdk2	Mybpc3	Rhag	Nhp2	Adra2a	Prkca	Rac2	Gimap4	Zfp57	Pmp22	Asb4	Lgr5	Leng8	Ssbp4
16	Ckap2l	Fga	Slu7	Pcdh7	Nrn1	Wnt5a	Hoxc5	Fgf18	Dmrt2	Med11	Slc15a2	Pxylp1	Jam2	Lix1	Rai2	Gm8113	Rrad	Rfesd	Gabra4	Pcyt1b	Gp5	Klk8	Prkcdbp	Fosl1	Tdo2	Tbx4	C330021F23Rik	Wars2	Rpl13
17	Apmap	Fabp2	B4galt3	Chpf	Plch1	Hoxa7	Mkln1os	Itpk1	Foxl2	Knop1	Wnt7a	Gabrg1	Arx	Lrrn3	Cmtm5	Edn3	Rbm24	Klf1	Gm26699	Gm14295	Slain2	Cyth4	Thsd1	Paqr5	Col1a1	Asb12	Ripply3	Nomo1	Rpl23
18	Leo1	Ass1	Fam20c	Chrd	Fam13a	Pabpc1	Zfp61	S1pr5	Saa2	Lmo1	Slc39a2	Nell2	Cdh20	Hes3	Cnmd	Otor	Mylk3	Cfap57	Nle1	Gml2	Unc119	Gimap1	Prkch	Ier3	Dcn	Pde9a	Tmem59l	Hsd17b2	Rpl37a
19	Rela	Gjb2	Errfi1	Gm16536	Gm45060	Gm53	Gm20666	Pcdh8	Serpinf1	Lsm6	Aqp4	Kbtbd11	Pou3f4	Dqx1	Fam81a	Nhs	Smyd1	Slc25a21	Ppid	4930550C14Rik	Tspan32	Al467606	Cd38	Gm12408	Plagl1	Ppp1r14a	H2-Q4	5031439G07Rik	Eif3h
20	Borcs7	1700019B21Rik	Ext2	Igsf8	Gm28793	Fbxl14	Aars2	Tmem132c	Uncx	Trim27	Tmcc3	Lyrm1	Egr2	Hoxc4	Cnp	Cpa1	Asb2	Ncf4	Hspd1	Gm43154	Slc35d3	Mfng	Kcne3	Cdc42bpa	Ece1	Rgs5	Ces1d	Gtpbp8	Impdh2
21	Mcm10	Atp6v0a1	Rab6b	St6galnac3	Gm44029	Gnal	Ibsp	Gzmk	Sncaip	Smu1	Efna5	Shisa8	Dmbx1	Ust	Sppl2b	Isl1	Apobec2	Mrap	Rpia	Ubash3a	Dapp1	Cxcr3	Klhl4	Nrp2	Akr1b8	Oxct1	Tmem200c	Bbs5	Rps27
22	Rapgef1	Cideb	Olfm1	Otud1	Krt33a	Pclaf	Proser1	Fam120b	Vegfd	Skiv2l2	Sptlc3	Tshz1	Samd5	Stk32c	L1cam	Hmgb1	Myh6	Hbq1b	Gpatch4	Lrrc57	Nrgn	Fcgr3	Plxnd1	Slc1a2	Fam162b	Hoxc10	Btnl9	Lrrc51	Rpl28
23	Krt2b	Slc22a18	Stag1	Elavl4	Gm15222	Fgf8	CT009486.1	Col13a1	Hlf	Cops4	Chst5	Msmo1	Apc2	Fam131b	Mcc	Clvs2	Ccdc141	Dhrs11	Gemin6	Fbf1	Sla2	Myd88	Ecscr	Galnt18	Fam114a1	Tbx2	Lamb3	Dis3l	Sct
24	Slmap	Dgat2	Tceal9	Fbxo25	Tgm3	Rspo3	Cntd1	4930458D05Rik	Pax1	Sf3b4	Elf5	Hes5	Pcsk2os1	Pde1a	Enpp2	Hotairm1	Bves	Asb17os	Mrpl18	Rpl13a	Mdm1	Cebpb	Esam	Enc1	Steap2	Efnb3	Cftr	Pde5a	Rpl32
25	Fut8	Sec14l2	Spink1	Htra1	Naa35	Stmn2	Zfp638	Lfng	Cped1	Six3	Krt23	Fndc5	Gpr162	Fam13c	Sphk1	Hdgfrp3	Ankrd1	Dapk2	Eif2b1	Eif1ad	Fyb	Prpf38b	Fam171a2	Kctd12b	Bmp4	Mettl7a1	Pcsk6	Lpar2	Rpl24

mRNA expression

gene	Up in WT
gene	Up in *Commd10*^{Null}

Neurogenesis

Heart development

Figure 5. Tissue distribution of differentially expressed genes in *Commd10*^{Null} embryos on E8.5. The top row of table lists 29 cell lineages/tissues present in normal mouse embryos at the E8.5 stage of embryogenesis. The columns list the top 25 lineage-specific gene markers for each tissue. All lists were found on a single-cell molecular map of mouse gastrulation and early organogenesis. at https://marionilab.cruk.cam.ac.uk/MouseGastrulation2018/ (accessed on 22 October 2022) website. Genes that are significantly expressed at lower levels in *Commd10*^{Null} embryos when compared with WT are shaded in red. Genes with higher expression in *Commd10*^{Null} are shaded in yellow. Blue and green brackets below the table mark cell lineages/tissues involved in neurogenesis and heart development, respectively.

In contrast to *Commd10*^{Null} embryos, *Commd9*$^{-/-}$ embryos die by E13.5 [56]. The authors found low levels of Hey1, Hey2, and Hes1 mRNA in the hearts of *Commd9*$^{-/-}$ embryos and concluded that the embryonic lethality of these mice was due to complex cardiovascular changes with signs of Notch deficiency. There were no differences in the mRNA expression of Notch or the genes listed above in *Commd10*^{Null} embryos compared with WT. Taken together, these data indicate that COMMD1-, COMMD9-, and COMMD10-deficient mice display different underlying reasons for failed embryonic development and suggest that COMMD proteins play different critical roles during embryogenesis.

No direct connection between COMMD10 and Sox10 has been described in the scientific literature. We can only speculate as to how the absence of COMMD10 may lead to lower expression of Sox10 and, sequentially, other genes during embryogenesis. During normal embryogenesis, Sox10 mRNA appears in late gastrulating embryos (mouse E7.5) in the neural crest-forming region, and its gene expression depends on Wnt signaling [57,58]. Sox10 protein was also found to directly interact with β-catenin [59], which is activated in the canonical Wnt signaling pathway (reviewed in [60]). Wnt protein ligands bind to Frizzled family receptors (cell surface Fzd proteins and co-receptor Lrp5/6). *Commd10*^{Null} embryos show significantly lower expression of Fzd3 and Fzd9 suggesting lower Wnt signaling potency. In addition, several Wnt ligands themselves were also dysregulated. There were higher levels of Wnt3 and Wnt9b while there were significantly lower levels of Wnt1,

Wnt7a, and Wnt8b, suggesting dysregulation of Wnt signaling pathways in *Commd10*^{Null} embryos. Wnt1-deficient mice exhibit a range of phenotypes, from early embryonic lethality to survival with severe ataxia [61]. Wnt7a signaling also controls multiple steps of neurogenesis [62]. It is plausible that by being part of the endosomal trafficking process inside the cell, COMMD10 may be involved in Wnt signaling regulation through as yet unknown mechanisms of Fzd receptor recycling or Wnt ligand secretion.

4. Limitations of the Study

The results described here characterize the timing of embryonic lethality of *Commd10*^{Null} mice and also begin to demonstrate that neural plate developmental delay is the most likely cause of *Commd10*^{Null} failed embryogenesis. The differential gene expression profile of *Commd10*^{Null} as compared to normally developing WT embryos after E8.5 does not necessarily imply direct associations with COMMD10 deficiency. They rather verify the timing of embryonic failure by E8.5. Broader approaches and detailed analyses of earlier embryos are needed to pinpoint the exact role of COMMD10 in mouse embryogenesis, which are subjects of continued study and outside the scope of the present study.

5. Conclusions

Our study demonstrated that COMMD10 deficiency leads to embryonic lethality by day E8.5, most likely due to impaired neural plate and neural crest development processes resulting from the decreased expression of transcription factor Sox10 and several other genes. The molecular mechanism by which COMMD10 upregulates *Sox10* expression remains unknown and merits further investigation.

Supplementary Materials: The following supporting information can be downloaded at: https://www.mdpi.com/article/10.3390/jdb11010013/s1, Figure S1: Complementary information for main figures; Supplementary Tables: GO:Biological Process of the top 15 genes upregulated in *Commd10*^{Null} embryos and the GO:Biological Process of the top 20 genes downregulated in *Commd10*^{Null} embryos; and a document with Supplementary figure titles and legends.

Author Contributions: Conceptualization, E.N.T. and I.F.D.; methodology, K.P.P., P.P. and G.W.; formal analysis, C.L. and M.B.; investigation, K.P.P., E.N.T., P.P. and A.V.T.; resources, I.F.D.; data curation, M.B.; writing—original draft preparation, A.V.T.; writing—review and editing, E.N.T., P.P., K.P.P. and I.F.D. All authors have read and agreed to the published version of the manuscript.

Funding: This work was carried out with help by the Oklahoma Medical Research Foundation Quantitative Analysis Core and supported by COBRE grant 1 P30 GM110766-01. The content is solely the responsibility of the authors and does not necessarily represent the official views of the National Institutes of Health.

Institutional Review Board Statement: All housing and experimental use of mice were carried out at AAALAC-accredited facility in accordance with United States federal, state, local, and institutional regulations and guidelines governing the use of animals and were approved by OUHSC Institutional Animal Care and Use Committee (animal study protocol No. 20-028, approval date 8 May 2020).

Informed Consent Statement: Not applicable.

Data Availability Statement: Most data generated or analyzed during this study are included in this published article and its Supplementary Materials. Unprocessed RNA-seq raw data files and processed data files have been deposited on NCBI Gene Expression Omnibus (https://www.ncbi.nlm.nih.gov/geo/query/acc.cgi?acc=GSE216492 (accessed on 13 March 2023). Further information and requests for materials should be directed to and will be fulfilled by the lead contact, Ian F. Dunn (ian-dunn@ouhsc.edu).

Acknowledgments: The authors thank Kathy J. Kyler for editing the manuscript, Hannah B. Homburg for assistance with mice, and Meng-Ling Wu for technical help with embryonic dissection techniques.

Conflicts of Interest: The authors declare no conflict of interest.

References

1. Chen, K.E.; Healy, M.D.; Collins, B.M. Towards a molecular understanding of endosomal trafficking by Retromer and Retriever. *Traffic* **2019**, *20*, 465–478. [CrossRef] [PubMed]
2. Phillips-Krawczak, C.A.; Singla, A.; Starokadomskyy, P.; Deng, Z.; Osborne, D.G.; Li, H.; Dick, C.J.; Gomez, T.S.; Koenecke, M.; Zhang, J.S.; et al. COMMD1 is linked to the WASH complex and regulates endosomal trafficking of the copper transporter ATP7A. *Mol. Biol. Cell* **2015**, *26*, 91–103. [CrossRef] [PubMed]
3. Bartuzi, P.; Billadeau, D.D.; Favier, R.; Rong, S.; Dekker, D.; Fedoseienko, A.; Fieten, H.; Wijers, M.; Levels, J.H.; Huijkman, N.; et al. CCC- and WASH-mediated endosomal sorting of LDLR is required for normal clearance of circulating LDL. *Nat. Commun.* **2016**, *7*, 10961. [CrossRef]
4. Qureshi, Y.H.; Baez, P.; Reitz, C. Endosomal Trafficking in Alzheimer's Disease, Parkinson's Disease, and Neuronal Ceroid Lipofuscinosis. *Mol. Cell. Biol.* **2020**, *40*, e00262-20. [CrossRef]
5. Mallam, A.L.; Marcotte, E.M. Systems-wide Studies Uncover Commander, a Multiprotein Complex Essential to Human Development. *Cell Syst.* **2017**, *4*, 483–494. [CrossRef]
6. Buckley, C.M.; Gopaldass, N.; Bosmani, C.; Johnston, S.A.; Soldati, T.; Insall, R.H.; King, J.S. WASH drives early recycling from macropinosomes and phagosomes to maintain surface phagocytic receptors. *Proc. Natl. Acad. Sci. USA* **2016**, *113*, E5906–E5915. [CrossRef]
7. King, J.S.; Gueho, A.; Hagedorn, M.; Gopaldass, N.; Leuba, F.; Soldati, T.; Insall, R.H. WASH is required for lysosomal recycling and efficient autophagic and phagocytic digestion. *Mol. Biol. Cell* **2013**, *24*, 2714–2726. [CrossRef] [PubMed]
8. Maine, G.N.; Burstein, E. COMMD proteins: COMMing to the scene. *Cell. Mol. Life Sci.* **2007**, *64*, 1997–2005. [CrossRef]
9. van De Sluis, B.; Rothuizen, J.; Pearson, P.L.; van Oost, B.A.; Wijmenga, C. Identification of a new copper metabolism gene by positional cloning in a purebred dog population. *Hum. Mol. Genet.* **2002**, *11*, 165–173. [CrossRef]
10. Muller, P.A.; van de Sluis, B.; Groot, A.J.; Verbeek, D.; Vonk, W.I.; Maine, G.N.; Burstein, E.; Wijmenga, C.; Vooijs, M.; Reits, E.; et al. Nuclear-cytosolic transport of COMMD1 regulates NF-kappaB and HIF-1 activity. *Traffic* **2009**, *10*, 514–527. [CrossRef]
11. Maine, G.N.; Mao, X.; Komarck, C.M.; Burstein, E. COMMD1 promotes the ubiquitination of NF-kappaB subunits through a cullin-containing ubiquitin ligase. *EMBO J.* **2007**, *26*, 436–447. [CrossRef]
12. Mouhadeb, O.; Ben Shlomo, S.; Cohen, K.; Farkash, I.; Gruber, S.; Maharshak, N.; Halpern, Z.; Burstein, E.; Gluck, N.; Varol, C. Impaired COMMD10-Mediated Regulation of Ly6C(hi) Monocyte-Driven Inflammation Disrupts Gut Barrier Function. *Front. Immunol.* **2018**, *9*, 2623. [CrossRef] [PubMed]
13. Ben Shlomo, S.; Mouhadeb, O.; Cohen, K.; Varol, C.; Gluck, N. COMMD10-Guided Phagolysosomal Maturation Promotes Clearance of Staphylococcus aureus in Macrophages. *iScience* **2019**, *14*, 147–163. [CrossRef] [PubMed]
14. Burstein, E.; Hoberg, J.E.; Wilkinson, A.S.; Rumble, J.M.; Csomos, R.A.; Komarck, C.M.; Maine, G.N.; Wilkinson, J.C.; Mayo, M.W.; Duckett, C.S. COMMD proteins, a novel family of structural and functional homologs of MURR1. *J. Biol. Chem.* **2005**, *280*, 22222–22232. [CrossRef]
15. Fan, Y.; Zhang, L.; Sun, Y.; Yang, M.; Wang, X.; Wu, X.; Huang, W.; Chen, L.; Pan, S.; Guan, J. Expression profile and bioinformatics analysis of COMMD10 in BALB/C mice and human. *Cancer Gene Ther.* **2020**, *27*, 216–225. [CrossRef]
16. Goodwin, L.O.; Splinter, E.; Davis, T.L.; Urban, R.; He, H.; Braun, R.E.; Chesler, E.J.; Kumar, V.; van Min, M.; Ndukum, J.; et al. Large-scale discovery of mouse transgenic integration sites reveals frequent structural variation and insertional mutagenesis. *Genome Res.* **2019**, *29*, 494–505. [CrossRef]
17. Bushnell, B. BBtools. Available online: http://sourceforge.net/projects/bbmap/ (accessed on 2 February 2022).
18. Dobin, A.; Davis, C.A.; Schlesinger, F.; Drenkow, J.; Zaleski, C.; Jha, S.; Batut, P.; Chaisson, M.; Gingeras, T.R. STAR: Ultrafast universal RNA-seq aligner. *Bioinformatics* **2013**, *29*, 15–21. [CrossRef]
19. Durinck, S.; Spellman, P.T.; Birney, E.; Huber, W. Mapping identifiers for the integration of genomic datasets with the R/Bioconductor package biomaRt. *Nat. Protoc.* **2009**, *4*, 1184–1191. [CrossRef] [PubMed]
20. Love, M.I.; Huber, W.; Anders, S. Moderated estimation of fold change and dispersion for RNA-seq data with DESeq2. *Genome Biol.* **2014**, *15*, 550. [CrossRef]
21. de Boer, J.; Williams, A.; Skavdis, G.; Harker, N.; Coles, M.; Tolaini, M.; Norton, T.; Williams, K.; Roderick, K.; Potocnik, A.J.; et al. Transgenic mice with hematopoietic and lymphoid specific expression of Cre. *Eur. J. Immunol.* **2003**, *33*, 314–325. [CrossRef]
22. Pijuan-Sala, B.; Griffiths, J.A.; Guibentif, C.; Hiscock, T.W.; Jawaid, W.; Calero-Nieto, F.J.; Mulas, C.; Ibarra-Soria, X.; Tyser, R.C.V.; Ho, D.L.L.; et al. A single-cell molecular map of mouse gastrulation and early organogenesis. *Nature* **2019**, *566*, 490–495. [CrossRef]
23. Pingault, V.; Zerad, L.; Bertani-Torres, W.; Bondurand, N. SOX10: 20 years of phenotypic plurality and current understanding of its developmental function. *J. Med. Genet.* **2022**, *59*, 105–114. [CrossRef]
24. Zhao, F.; Satoda, M.; Licht, J.D.; Hayashizaki, Y.; Gelb, B.D. Cloning and characterization of a novel mouse AP-2 transcription factor, AP-2delta, with unique DNA binding and transactivation properties. *J. Biol. Chem.* **2001**, *276*, 40755–40760. [CrossRef] [PubMed]
25. Zhao, F.; Bosserhoff, A.K.; Buettner, R.; Moser, M. A heart-hand syndrome gene: Tfap2b plays a critical role in the development and remodeling of mouse ductus arteriosus and limb patterning. *PLoS ONE* **2011**, *6*, e22908. [CrossRef]
26. Zhou, C.; Tsai, S.Y.; Tsai, M.J. COUP-TFI: An intrinsic factor for early regionalization of the neocortex. *Genes Dev.* **2001**, *15*, 2054–2059. [CrossRef] [PubMed]

27. Mehra-Chaudhary, R.; Matsui, H.; Raghow, R. Msx3 protein recruits histone deacetylase to down-regulate the Msx1 promoter. *Biochem. J.* **2001**, *353*, 13–22. [CrossRef]
28. Zuber, M.E.; Gestri, G.; Viczian, A.S.; Barsacchi, G.; Harris, W.A. Specification of the vertebrate eye by a network of eye field transcription factors. *Development* **2003**, *130*, 5155–5167. [CrossRef]
29. Takahashi, M.; Osumi, N. Pax6 regulates specification of ventral neurone subtypes in the hindbrain by establishing progenitor domains. *Development* **2002**, *129*, 1327–1338. [CrossRef] [PubMed]
30. Zhao, Y.; Matsuo-Takasaki, M.; Tsuboi, I.; Kimura, K.; Salazar, G.T.; Yamashita, T.; Ohneda, O. Dual functions of hypoxia-inducible factor 1 alpha for the commitment of mouse embryonic stem cells toward a neural lineage. *Stem Cells Dev.* **2014**, *23*, 2143–2155. [CrossRef]
31. Zhang, Y.B.; Hu, J.; Zhang, J.; Zhou, X.; Li, X.; Gu, C.; Liu, T.; Xie, Y.; Liu, J.; Gu, M.; et al. Genome-wide association study identifies multiple susceptibility loci for craniofacial microsomia. *Nat. Commun.* **2016**, *7*, 10605. [CrossRef] [PubMed]
32. Aruga, J.; Tohmonda, T.; Homma, S.; Mikoshiba, K. Zic1 promotes the expansion of dorsal neural progenitors in spinal cord by inhibiting neuronal differentiation. *Dev. Biol.* **2002**, *244*, 329–341. [CrossRef]
33. Wapinski, O.L.; Vierbuchen, T.; Qu, K.; Lee, Q.Y.; Chanda, S.; Fuentes, D.R.; Giresi, P.G.; Ng, Y.H.; Marro, S.; Neff, N.F.; et al. Hierarchical mechanisms for direct reprogramming of fibroblasts to neurons. *Cell* **2013**, *155*, 621–635. [CrossRef]
34. Vierbuchen, T.; Ostermeier, A.; Pang, Z.P.; Kokubu, Y.; Südhof, T.C.; Wernig, M. Direct conversion of fibroblasts to functional neurons by defined factors. *Nature* **2010**, *463*, 1035–1041. [CrossRef]
35. Treutlein, B.; Lee, Q.Y.; Camp, J.G.; Mall, M.; Koh, W.; Shariati, S.A.; Sim, S.; Neff, N.F.; Skotheim, J.M.; Wernig, M.; et al. Dissecting direct reprogramming from fibroblast to neuron using single-cell RNA-seq. *Nature* **2016**, *534*, 391–395. [CrossRef]
36. Whittaker, D.E.; Oleari, R.; Gregory, L.C.; Le Quesne-Stabej, P.; Williams, H.J.; Torpiano, J.G.; Formosa, N.; Cachia, M.J.; Field, D.; Lettieri, A.; et al. A recessive PRDM13 mutation results in congenital hypogonadotropic hypogonadism and cerebellar hypoplasia. *J. Clin. Investig.* **2021**, *131*, e141587. [CrossRef]
37. Hirata, T.; Nakazawa, M.; Yoshihara, S.; Miyachi, H.; Kitamura, K.; Yoshihara, Y.; Hibi, M. Zinc-finger gene Fez in the olfactory sensory neurons regulates development of the olfactory bulb non-cell-autonomously. *Development* **2006**, *133*, 1433–1443. [CrossRef]
38. Jean, D.; Bernier, G.; Gruss, P. Six6 (Optx2) is a novel murine Six3-related homeobox gene that demarcates the presumptive pituitary/hypothalamic axis and the ventral optic stalk. *Mech. Dev.* **1999**, *84*, 31–40. [CrossRef] [PubMed]
39. Toy, J.; Yang, J.M.; Leppert, G.S.; Sundin, O.H. The optx2 homeobox gene is expressed in early precursors of the eye and activates retina-specific genes. *Proc. Natl. Acad. Sci. USA* **1998**, *95*, 10643–10648. [CrossRef]
40. Marçal, N.; Patel, H.; Dong, Z.; Belanger-Jasmin, S.; Hoffman, B.; Helgason, C.D.; Dang, J.; Stifani, S. Antagonistic effects of Grg6 and Groucho/TLE on the transcription repression activity of brain factor 1/FoxG1 and cortical neuron differentiation. *Mol. Cell. Biol.* **2005**, *25*, 10916–10929. [CrossRef] [PubMed]
41. Wijchers, P.J.; Hoekman, M.F.; Burbach, J.P.; Smidt, M.P. Cloning and analysis of the murine Foxi2 transcription factor. *Biochim. Biophys. Acta* **2005**, *1731*, 133–138. [CrossRef] [PubMed]
42. Hienola, A.; Pekkanen, M.; Raulo, E.; Vanttola, P.; Rauvala, H. HB-GAM inhibits proliferation and enhances differentiation of neural stem cells. *Mol. Cell. Neurosci.* **2004**, *26*, 75–88. [CrossRef]
43. Zou, P.; Muramatsu, H.; Sone, M.; Hayashi, H.; Nakashima, T.; Muramatsu, T. Mice doubly deficient in the midkine and pleiotrophin genes exhibit deficits in the expression of beta-tectorin gene and in auditory response. *Lab. Investig.* **2006**, *86*, 645–653. [CrossRef]
44. Nakamura, E.; Kadomatsu, K.; Yuasa, S.; Muramatsu, H.; Mamiya, T.; Nabeshima, T.; Fan, Q.W.; Ishiguro, K.; Igakura, T.; Matsubara, S.; et al. Disruption of the midkine gene (Mdk) resulted in altered expression of a calcium binding protein in the hippocampus of infant mice and their abnormal behaviour. *Genes Cells* **1998**, *3*, 811–822. [CrossRef]
45. Khokha, M.K.; Hsu, D.; Brunet, L.J.; Dionne, M.S.; Harland, R.M. Gremlin is the BMP antagonist required for maintenance of Shh and Fgf signals during limb patterning. *Nat. Genet.* **2003**, *34*, 303–307. [CrossRef] [PubMed]
46. Mankoo, B.S.; Skuntz, S.; Harrigan, I.; Grigorieva, E.; Candia, A.; Wright, C.V.; Arnheiter, H.; Pachnis, V. The concerted action of Meox homeobox genes is required upstream of genetic pathways essential for the formation, patterning and differentiation of somites. *Development* **2003**, *130*, 4655–4664. [CrossRef] [PubMed]
47. Paththinige, C.S.; Sirisena, N.D.; Escande, F.; Manouvrier, S.; Petit, F.; Dissanayake, V.H.W. Split hand/foot malformation with long bone deficiency associated with BHLHA9 gene duplication: A case report and review of literature. *BMC Med Genet.* **2019**, *20*, 108. [CrossRef] [PubMed]
48. Klopocki, E.; Lohan, S.; Doelken, S.C.; Stricker, S.; Ockeloen, C.W.; Soares Thiele de Aguiar, R.; Lezirovitz, K.; Mingroni Netto, R.C.; Jamsheer, A.; Shah, H.; et al. Duplications of BHLHA9 are associated with ectrodactyly and tibia hemimelia inherited in non-Mendelian fashion. *J. Med Genet.* **2012**, *49*, 119–125. [CrossRef]
49. Patel, D.M.; Ahmad, S.F.; Weiss, D.G.; Gerke, V.; Kuznetsov, S.A. Annexin A1 is a new functional linker between actin filaments and phagosomes during phagocytosis. *J. Cell Sci.* **2011**, *124*, 578–588. [CrossRef]
50. Blaybel, R.; Théoleyre, O.; Douablin, A.; Baklouti, F. Downregulation of the Spi-1/PU.1 oncogene induces the expression of TRIM10/HERF1, a key factor required for terminal erythroid cell differentiation and survival. *Cell Res.* **2008**, *18*, 834–845. [CrossRef]
51. Yang, H.; Wang, X.X.; Zhou, C.Y.; Xiao, X.; Tian, C.; Li, H.H.; Yin, C.L.; Wang, H.X. Tripartite motif 10 regulates cardiac hypertrophy by targeting the PTEN/AKT pathway. *J. Cell. Mol. Med.* **2020**, *24*, 6233–6241. [CrossRef]

52. Tang, W.; Martik, M.L.; Li, Y.; Bronner, M.E. Cardiac neural crest contributes to cardiomyocytes in amniotes and heart regeneration in zebrafish. *eLife* **2019**, *8*, e47929. [CrossRef] [PubMed]
53. Abdul-Wajid, S.; Demarest, B.L.; Yost, H.J. Loss of embryonic neural crest derived cardiomyocytes causes adult onset hypertrophic cardiomyopathy in zebrafish. *Nat. Commun.* **2018**, *9*, 4603. [CrossRef] [PubMed]
54. Chen, J.; Bardes, E.E.; Aronow, B.J.; Jegga, A.G. ToppGene Suite for gene list enrichment analysis and candidate gene prioritization. *Nucleic Acids Res.* **2009**, *37*, W305–W311. [CrossRef]
55. van de Sluis, B.; Muller, P.; Duran, K.; Chen, A.; Groot, A.J.; Klomp, L.W.; Liu, P.P.; Wijmenga, C. Increased activity of hypoxia-inducible factor 1 is associated with early embryonic lethality in Commd1 null mice. *Mol. Cell. Biol.* **2007**, *27*, 4142–4156. [CrossRef] [PubMed]
56. Li, H.; Koo, Y.; Mao, X.; Sifuentes-Dominguez, L.; Morris, L.L.; Jia, D.; Miyata, N.; Faulkner, R.A.; van Deursen, J.M.; Vooijs, M.; et al. Endosomal sorting of Notch receptors through COMMD9-dependent pathways modulates Notch signaling. *J. Cell Biol.* **2015**, *211*, 605–617. [CrossRef]
57. Bhattarai, C.; Poudel, P.P.; Ghosh, A.; Kalthur, S.G. Comparative role of SOX10 gene in the gliogenesis of central, peripheral, and enteric nervous systems. *Differentiation* **2022**, *128*, 13–25. [CrossRef]
58. Sutton, G.; Kelsh, R.N.; Scholpp, S. Review: The Role of Wnt/β-Catenin Signalling in Neural Crest Development in Zebrafish. *Front. Cell Dev. Biol.* **2021**, *9*, 782445. [CrossRef]
59. Uka, R.; Britschgi, C.; Krättli, A.; Matter, C.; Mihic, D.; Okoniewski, M.J.; Gualandi, M.; Stupp, R.; Cinelli, P.; Dummer, R.; et al. Temporal activation of WNT/β-catenin signaling is sufficient to inhibit SOX10 expression and block melanoma growth. *Oncogene* **2020**, *39*, 4132–4154. [CrossRef]
60. Zhong, Z.A.; Michalski, M.N.; Stevens, P.D.; Sall, E.A.; Williams, B.O. Regulation of Wnt receptor activity: Implications for therapeutic development in colon cancer. *J. Biol. Chem.* **2021**, *296*, 100782. [CrossRef]
61. Thomas, K.R.; Capecchi, M.R. Targeted disruption of the murine int-1 proto-oncogene resulting in severe abnormalities in midbrain and cerebellar development. *Nature* **1990**, *346*, 847–850. [CrossRef]
62. Qu, Q.; Sun, G.; Murai, K.; Ye, P.; Li, W.; Asuelime, G.; Cheung, Y.T.; Shi, Y. Wnt7a regulates multiple steps of neurogenesis. *Mol. Cell. Biol.* **2013**, *33*, 2551–2559. [CrossRef] [PubMed]